Optical microlinear accelerator for molecules and atoms

P. F. Barker
The Department of Physics, Heriot-Watt University, Edinburgh, EH14 4AS, Scotland

M. N. Shneider
Department of Mechanical and Aerospace Engineering, Princeton University, Princeton, New Jersey 08544
(Received 18 January 2001; published 6 August 2001)

The traveling periodic dipole potential of an accelerated optical lattice, created by high-intensity short-pulse lasers, can accelerate polarizable atoms and molecules that are initially at room temperature to hyperthermal velocities (10–100 km/s). We study the acceleration of trapped and untrapped ensembles of particles and show that a significant fraction (30%) of uniformly distributed particles can be accelerated to high velocities over micron-size distances, within nanosecond and subnanosecond time scales.

DOI: 10.1103/PhysRevA.64.033408 PACS number(s): 32.80.Lg, 42.50.Vk, 51.10.+y

I. INTRODUCTION

Synchronous acceleration of charged particles to energies in excess of 100 GeV can be achieved using electrostatic and Lorentz forces, and accelerated neutral atomic beams can be created from ion beams by charge capture [1]. Gas dynamic methods that accelerate molecules to greater than 10 km/s (14.5 eV for N_2) [2] have been demonstrated, but to our knowledge no method has been demonstrated that can accelerate neutral molecules above this energy range without a large fraction of the gas being thermally ionized and dissociated [3].

Recently, synchronous deceleration of dipolar molecules using time-dependent stark forces has been demonstrated [4–6]. In this technique, polar molecules are trapped and decelerated in a stark potential created by an electrostatic traveling wave produced by up to 68 electrode stages. This scheme was used to decelerate jet-cooled molecules moving at supersonic speeds to near zero velocity. For the case of ND_3, a density of 10^6 cm^{-3} was decelerated to zero velocity in the laboratory frame and trapped electrostatically. As pointed out by the authors, this concept could also be used to accelerate dipolar molecules to high energy and velocity, in analogy to the synchronous acceleration of charged particle accelerators.

Linear acceleration within the time-varying electric field of an accelerated optical traveling wave has been proposed as a means to accelerate atoms to high velocity [7,8] and more recently molecular acceleration has been proposed [9,10]. Rotational acceleration of trapped molecules using chirped fields has already been demonstrated, and centrifugal dissociation has been achieved [11]. Linear acceleration using optical fields is attractive because extremely large dipole forces can be produced by the high electric field gradients that can be created within an optical traveling wave. The electrodeless electric field gradient produced by a focused laser beam can be orders of magnitude greater than electrostatic gradients, allowing acceleration of not only polar, but also polarizable molecules and atoms. This concept has already been demonstrated with acceleration of ultracold atoms up to the velocities in the m/s range using very weak optical periodic potentials, which are called optical lattices [12,13]. A one-dimensional optical lattice is created by two counterpropagating laser beams, and acceleration of the lattice is achieved by changing the frequency of the counter propagating fields (chirping) with respect to time.

In contrast to acceleration of ultracold atoms in weak lattices [12,13], we study the acceleration of polarizable gas particles, such as molecules and atoms at much higher temperatures (5–300 K), to velocities in the 10–100 km/s range by application of large lattice potentials created by pulsed lasers. Our work follows on from the original work of Kazantsev [7,8], and investigates the motion of trapped and untrapped particles in the velocity phase space of the accelerated dipole potential. We study the dynamics of the accelerating ensemble of polarizable particles under the influence of large dipole or stark forces, and predict the velocity distribution function of both trapped and untrapped particles.

II. DIPOLE FORCE IN A LATTICE

The force that can be applied to a polarizable particle depends on its mass m, polarizability α, and the strength of the applied external electric field $E(x,t)$. For a polarizable particle, far from resonance, the dipole force or electrostrictive force within a standing or slowly traveling optical wave in one dimension is given by [14]:

$$F(x,t)=\frac{1}{2}\alpha\nabla E(x,t)^2. \tag{1}$$

The polarizability of a molecule that is not aligned within the field is given by $\alpha=(\alpha_{\|}+2\alpha_{\perp})/3$, where $\alpha_{\|}$ and $\alpha_{\perp}$ are the parallel and perpendicular components of the static polarizability with respect to the molecular axis [15]. This expression is a lower limit to the force because, in an intense field, molecular alignment of the molecule with the field has been shown to occur when the pulse duration is greater than inverse of the rotational rate. This process increases the effective polarizability, and therefore the available force [16,17]. We consider an accelerating optical lattice that is formed by two almost counterpropagating fields denoted by subscripts 1 and 2, as shown in Fig. 1. The slowly varying square of the electric field that will lead to acceleration is

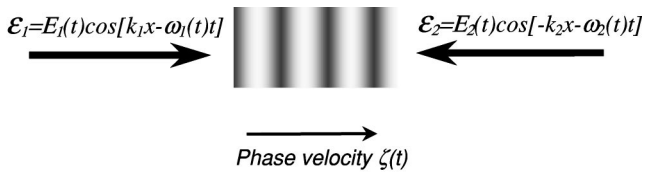

FIG. 1. The creation of an optical lattice by two counterpropagating optical fields for acceleration of molecules and atoms.

given by $E(x,t)^2=E_1(t)E_2(t)\cos(qx-\beta t^2)$, where $q=|k_1+k_2|$ is the wave number; and $\beta=d\omega(t)/dt$ is the frequency chirp due to the time-dependent frequency difference between each of the fields where $\omega(t)=\omega_1(t)-\omega_2(t)$. We require that $\omega(t)\ll\omega_1(t),\omega_2(t)$, and therefore q is approximately constant over the chirped frequency range. In Fig. 1, the instantaneous phase velocity is indicated for a positive chirp. The phase velocity $\zeta(t)$ of the lattice is given by

$$\zeta(t)=\frac{2\beta t}{q}. \tag{2}$$

This will also be the average velocity of a particle that is trapped and accelerated by the lattice. We consider acceleration of ensembles of ''hot'' particles that are initially at thermal equilibrium near room temperature, and do not consider the quantized motion of the particles. The equation of motion for a particle that is perturbed by the periodic potential of the optical lattice is derived from Eq. (1), and is given by $d^2x/dt^2=-\frac{1}{2}[\alpha qE_1(t)E_2(t)/m]\sin(qx-\beta t^2)$, where m is the mass of the accelerated particle. In a reference frame that accelerates with the optical lattice, this equation in nondimensional units, is now given by

$$\frac{d^2\theta}{dT^2}=-\frac{aq}{\beta}\sin\theta-2, \tag{3}$$

where $\theta=X-T^2$ is the phase of the particle with respect to the accelerated frame, and $T=\sqrt{\beta}t$ and $X=qx$ are the nondimensional temporal and spatial variables, respectively. The maximum force per unit mass supplied by the optical lattice is given by $a=\frac{1}{2}[\alpha qE_1(t)E_2(t)/m]$, and for most of this paper we assume that the electric field amplitudes are equal and constant in time, $E_1(t),E_2(t)=E_1,E_2$. We have assumed that the optical fields are sufficiently far detuned from resonance so that the force is harmonic [18]. Equation (3) is also the equation of motion for a pendulum under constant torque.

III. VELOCITY PHASE SPACE

The periodicity of an optical lattice is on the order of hundreds of nanometers, so it is necessary to consider the effect of the lattice potential on particles at all phases and all initial velocities because, unlike the macroscopic acceleration in electrostatic traveling potentials, particles cannot be injected into an optical lattice at the correct phase. To understand the motion of both trapped and untrapped particles within the lattice, it is instructive to investigate the trajectory

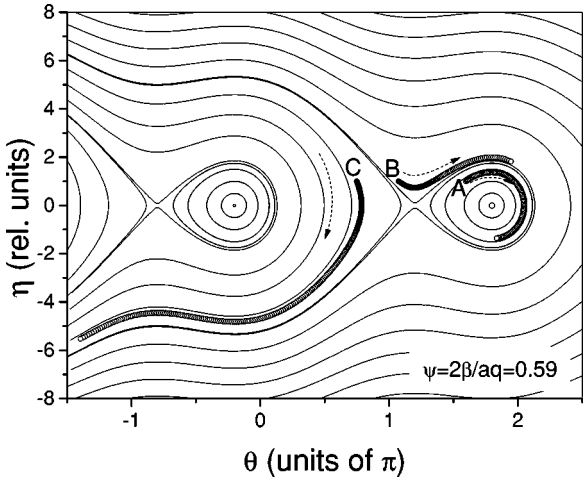

FIG. 2. The velocity phase-space diagram for trapped particles for the case $\psi=0.59$. The trajectories of three particles at the same initial velocity, but with different phases with respect to the equilibrium point at $[\theta,\eta]=[5.70,0.00]$ are shown. The horizontal axis corresponds to the phase in the accelerated frame θ, and the vertical axis to η, which is proportional to velocity given by $\beta^{1/2}/q\,\eta$.

of particles in the velocity phase space $[\eta,\theta]$, derived from Eq. (3). These system of equations is given by

$$\frac{d\eta}{dT}=-\frac{aq}{\beta}\sin\theta-2, \tag{4}$$

$$\frac{d\theta}{dT}=\eta. \tag{5}$$

We find the critical points of this system, as usual, by setting Eqs. (4) and (5) equal to zero. The critical points correspond to $\sin\theta=-2\beta/aq$, and $\eta=0$. A linear stability analysis of Eqs. (4) and (5) around the critical points indicate that the family of points $[\theta,\eta]=[2n\pi-\sin^{-1}\psi,0]$ are stable equilibrium points, where n is an integer and $\psi=2\beta/aq$. The points $[\theta,\eta]=[(2n-1)\pi+\sin^{-1}\psi,0]$ are unstable equilibrium or saddle points.

The velocity phase-space diagram for Eqs. (4) and (5) is shown in Fig. 2 for the case $\psi=0.59$. The horizontal axis corresponds to the phase in the accelerated frame θ, and the vertical axis to η, which is proportional to velocity given by $\sqrt{\beta}/q\,\eta$. The contours in the diagram correspond to the time-independent trajectory of particles in the η, θ phase-space diagram. A stationary particle that is not perturbed by the lattice potential would move in a parabolic trajectory centered on the θ axis. Shown on this diagram as open circles are the trajectories of three particles perturbed by the lattice. The trajectories are denoted by *A*, *B*, and *C*, and correspond to the motion of the particle for a time period $\Delta t=2.37/\sqrt{\beta}$. Each particle is initially at a different phase, but at the same velocity with $\eta=1.0$. Trajectory *A* corresponds to a particle that is initially 0.08 rad behind the equilibrium point $[\theta,\eta]=[5.70,0.00]$. Its trajectory indicates that it is trapped by the lattice and will orbit around the tear-drop-shaped equilibrium region infinitely, with a final velocity limited only by the

duration that the optical field can be maintained at the same intensity. The phase diagram demonstrates that, under collisionless conditions, a particle that is not initially trapped will never be trapped even though its motion can be strongly perturbed by the potential. Particle *B* is such an untrapped particle; it is initially 2.84 rad behind the same equilibrium point. Its motion is strongly perturbed by the potential, as evidenced by its trajectory in the phase plane around the tear-drop-shaped region of closed orbits. This particle initially moves towards the saddle point at $\theta=3.74$, but is deflected around the trapped region, briefly increasing its velocity with respect to the lattice velocity. For the short time period shown, the velocity of particle *B* is greater than the lattice velocity. However, because particle B is not trapped, its velocity would eventually decrease below that of the accelerated lattice, and thereafter its motion would not be strongly perturbed by the lattice. For short time periods, the acceleration of a distribution of untrapped particles with similar initial velocity and phase with respect to the lattice may constitute a significant proportion of an accelerated particle distribution. This type of acceleration is only significant on short time scales where the rate of acceleration and the potential are large enough to accelerate the particle to the required velocity before it completes its orbit around the tear-drop-shaped region of stability shown in Fig. 2. Particle *C* is initially 2.81 rad ahead of the equilibrium point at $\theta=-0.58$. It is not strongly perturbed by the lattice and follows an almost parabolic trajectory around the θ axis that is similar to an unperturbed trajectory.

IV. ACCELERATION OF TRAPPED PARTICLES

For a lattice with a stable equilibrium point, $\sin\theta=-\psi$ and therefore,

$$\left|\frac{2\beta}{aq}\right|<1 \tag{6}$$

is the condition for a particle to be trapped and accelerated by the lattice. This condition implies that the chirp β must be less than $aq/2$, and confirms the intuitive result that the acceleration of the lattice, $a_L=2\beta/q$, must be less than a, the maximum force per unit mass supplied by the gradient of the lattice potential. This requirement can be seen clearly from a diagram of the potential, $U(\theta)=-\int m/q^2 d^2\theta/dt^2 d\theta$, in the accelerated frame, as shown in Fig. 3. The location of the saddle point and equilibrium points, as determined from Eqs. (4) and (5) for $\psi=0.39$, 0.59, and 0.79 are shown. The depth of the potential well in each case is determined by the difference in potential height between a saddle point and its closest equilibrium point. The potential well depth, ΔU is given by

$$\Delta U=\frac{ma}{q}[2\cos(\sin^{-1}\psi)-\psi(\pi-2\sin^{-1}\psi)]. \tag{7}$$

It can be seen from Eq. (7) that no potential well exists for case $\psi\geqslant 1$, because either the chirp is too high, or the force per unit mass supplied by the lattice is not sufficient to trap

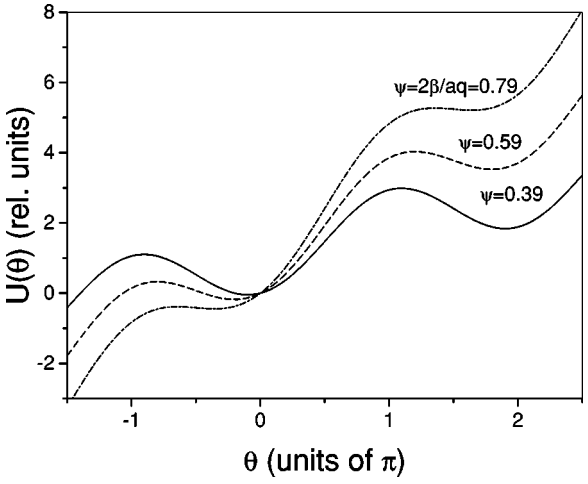

FIG. 3. The optical lattice potential, in the accelerated frame for $\psi=0.39,0.59,0.79$.

particles. The maximum well depth is given by $\Delta U_{\max}=2ma/q$ when $\psi=0$ that corresponds to the case with no chirp or acceleration. In the accelerated frame, any particle that is initially trapped in the potential well will remain in the well and oscillate about the stable critical point, $[\theta,\eta]=[2n\pi-\sin^{-1}\psi,0]$, with a characteristic frequency that depends on its initial phase and velocity. Acceleration without oscillation occurs only for particles initially at this critical point. The maximum velocity spread of the trapped and accelerated particles is given by

$$\Delta v=2\sqrt{\frac{2\Delta U}{m}}, \tag{8}$$

which determines the maximum velocity deviation that a trapped particle can attain in its oscillation around the stable equilibrium point. Figure 4 is a graph of particle velocity

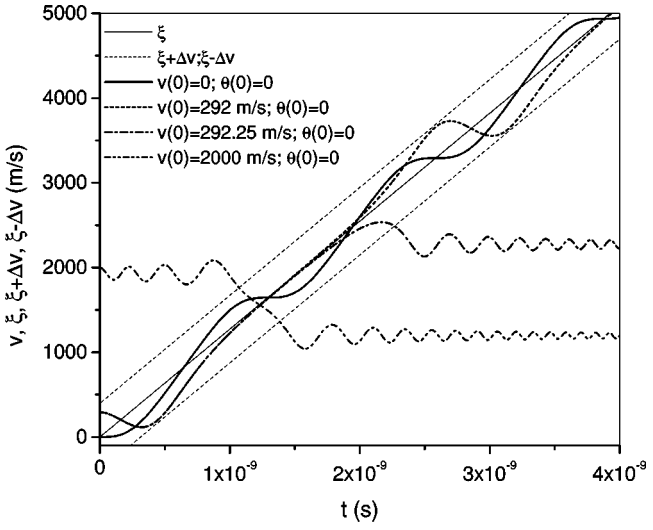

FIG. 4. A graph of velocity versus time for $\psi=0.59$. Each particle is initially at the same phase with respect to the lattice, but they have different initial velocities. The trapped particle velocity spread is indicated by the two parallel lines.

versus time in the laboratory frame that shows the evolution of the velocity of a number of particles perturbed by the lattice for the case of $\psi=0.59$ over a 4-ns time period. The particles are initially at different velocities, but at the same phase with respect to the initial lattice velocity at $v=0$ km/s. The particles with initial velocities of 0 and 292 m/s are trapped and can be accelerated indefinitely, with each particle oscillating at a different frequency around the lattice velocity. The velocity spread Δv of trapped and accelerated particles is indicated by the two parallel lines that bound the trajectories of the trapped particles. For a lattice with $\psi=0.59$, $a=2.14\times10^{12}$ m/s^2, $q=1.57\times10^{7}$ m^{-1}, where the electric field for each beam is $E_1=E_2=5\times10^{9}$ V/m, the potential well depth of $\Delta U\approx133$ K corresponds to a velocity spread of 735 m/s. The particle shown with an initial velocity of 292.25 m/s is accelerated by the potential for approximately 2 ns before being lost out of the lattice. This particle has a similar trajectory to particle *B* in Fig. 2, which only has one incomplete orbit around the equilibrium point before being lost from the lattice even though its initial velocity is less than $|\Delta v/2|$. Its final velocity is approximately 2.29 km/s that corresponds to an increase of almost 2 km/s within the 2-ns acceleration period. No particles with an initial velocity higher than $|\Delta v/2|$ are trapped and accelerated. Note that some particles are decelerated. The particle that is initially at 2 km/s is decelerated to 1.18 km/s, with most of this deceleration occurring over a 1-ns time period when the lattice velocity is close to the particle's initial velocity.

V. ACCELERATION OF AN ENSEMBLE OF PARTICLES

The evolution of particles that are distributed over a range of velocities, and over all phases, can be conveniently calculated from the collisionless Boltzmann equation given by [19,20]:

$$\frac{\partial f}{\partial t}+v\frac{\partial f}{\partial x}+\frac{F(x,t)}{m}\frac{\partial f}{\partial v}=\left(\frac{\partial f}{\partial t}\right)_c=0, \tag{9}$$

where $f=f(x,v,t)$ is the distribution function due to the optical perturbation, $(\partial f/\partial t)_c$ is the collision integral, and F is the external force defined earlier. For short acceleration periods, acceleration without collisions between particles becomes possible at pressures in the 100 torr range, and the collision integral can be set to zero. The maximum pressure for collisionless acceleration can be estimated from $p<2l_{m0}T_0/300a\tau^2$, where p is the pressure in torr, l_{m0} is the free-collision length at 1 torr and 300 K, and τ is the time of acceleration. To calculate the velocity distribution we assume, for simplicity, a periodic potential with infinite length. This condition elucidates the essential physics and allows the use of the cyclic boundary condition $f(-L/2,v,t)=f(L/2,v,t)$, where $L=2\lambda$, and where $\lambda=4\pi/q$ for counterpropagating beams. Equation (9) is also subject to the boundary conditions $f(x,v\rightarrow\pm\infty,t)=0$. Equation (9) was numerically integrated using a McCormack second-order finite-difference scheme [21], with an initial condition $f(x,v,t=0)=f_0(v,T_0)$, and where $f_0(v,T_0)$ is the equilibrium Maxwell-Boltzmann distribution at gas temperature T_0.

Figure 5 shows the evolution in time of an ensemble of thermally distributed CH_4 molecules, that are initially at temperature of $T_0=300$ K, and are perturbed by an accelerating optical lattice. The top hat temporal intensity profile is chosen so that the results can be compared with the velocity phase diagram of Fig. 2. The evolution of the initial Maxwell-Boltzmann distribution function is calculated by integration of Eq. (9), as discussed above. The distribution function is averaged over the spatial period of the lattice at each time. The top hat profile has the ratio $\psi=0.59$, which corresponds to a total laser intensity (both beams) of 6.5×10^{16} W/m^2 (6.5×10^{12} W/cm^2), and a chirp of 1×10^{19} rad/s^2. We use the static polarizability of CH_4, which is $\alpha=2.9\times10^{-40}$ Cm^2/V [22]. Figure 5 shows the evolution of the perturbed distribution, for each temporal profile, as the lattice is accelerated from an initial zero velocity. Approximately 30% of the particles are trapped and accelerated at the phase velocity, reaching 10.2 km/s in the 8 ns duration of the calculation. The long tail between the largely unperturbed distribution at $v=0$ m/s and the accelerated distribution is caused by molecules that are undergoing incomplete unstable orbits around the stable region in the phase space. After 2 ns, the number of particles in the accelerated distribution is approximately constant, indicating that the integration scheme is working correctly and that no particles are being numerically lost from the accelerated distribution. The velocity spread of the accelerated distribution after 2 ns is approximately 840 m/s, which is in good agreement with 735 m/s calculated from Eqs. (7) and (8). The larger velocity width of the calculated distribution can most probably be attributed to discretization error, and the tail of untrapped particles. This accelerated distribution is almost Gaussian with a full-width half-maximum velocity spread that corresponds to a temperature in the accelerated frame of 41 K. It is emphasized that the initial temperature of the ensemble does not determine the energy spread of the accelerated distribution, only the fraction that will be accelerated.

VI. ACCELERATION OF UNTRAPPED PARTICLES

A. $\psi<1$

Individual particles within an ensemble are distributed over all phases with respect to the initial lattice, but, as shown above, not all particles can be trapped by the potential, even if their kinetic energy is less than the potential well depth. Figure 6 is a time series that shows the temporal evolution of an ensemble of untrapped CH_4 molecules, like particle *B* in Fig. 2, that can be accelerated to velocities in km/s range. The CH_4 ensemble, initially at a temperature of 300 K, is perturbed by an optical lattice with $\psi=0.59$. As in Fig. 5, the velocity distribution at each time is calculated by numerical integration of Eq. (9). The constant $\psi=0.59$, is the same as for Fig. 5, but an initial lattice velocity of $\zeta(0)=-5$ km/s was chosen to be much greater than $|\Delta v/2|=368$ m/s, the velocity range for particles to be trapped. Figure 6 shows clearly that an accelerated distribution of untrapped molecules is produced at 4, 5, and 6 ns. At 4 ns, the peak of the accelerated distribution is centered at a velocity of approximately 600 m/s, which is much higher than

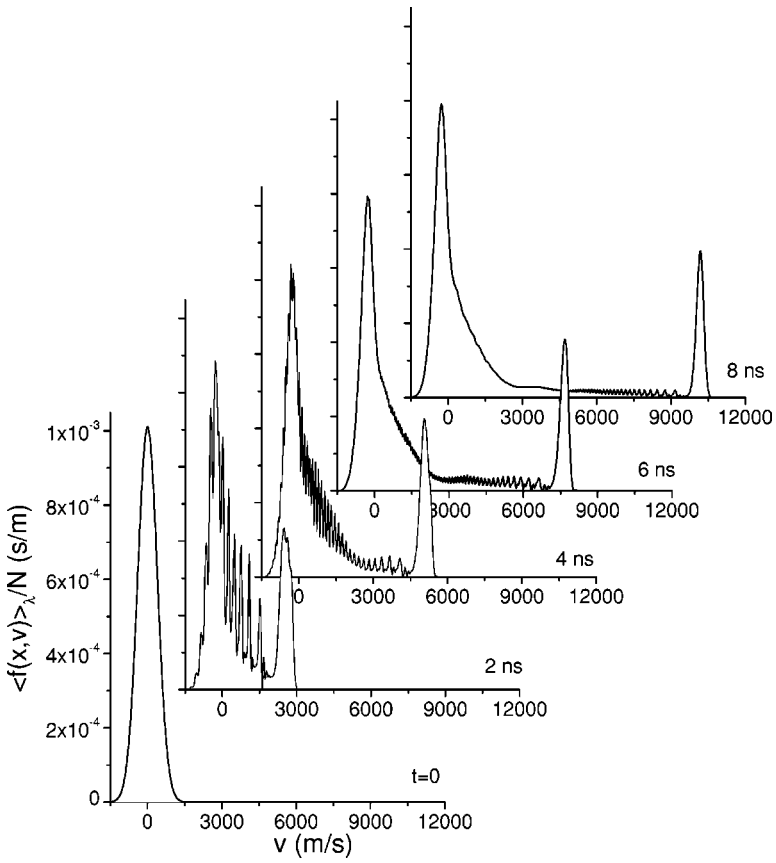

FIG. 5. The instantaneous velocity distribution function of CH_4 molecules within an accelerating optical lattice in 2-ns time increments after the lattice is created. The distribution function was averaged over the spatial period of the lattice and $\psi=0.59$.

the lattice velocity at 95 m/s. However, at 5 ns, the peak of the accelerated distribution is at lower velocity (1.1 km/s) than the lattice velocity of 1.36 km/s. At 6 ns the accelerated distribution is less well defined, but the velocity is approximately equal to the lattice velocity at 2.64 km/s. Unlike the accelerated distribution of trapped particles in Fig. 5, this accelerated distribution is not well defined because particles are no longer significantly accelerated after they complete their single orbit around the stable region shown in Fig. 2.

B. $\psi \geqslant 1$

Thus far we have concentrated on acceleration of both trapped and untrapped particles in an optical potential where a stable equilibrium exists. If the lattice acceleration or frequency chirp is too rapid, or the force of the lattice is not sufficient to trap particles, $\psi=2\beta/aq>1$, and a stable equilibrium no longer exists. Although particles can no longer be trapped or accelerated in a well-defined distribution, they can still be accelerated and decelerated in the lattice because the potential is periodically modulated. The velocity phase-space diagram for the case $\psi=2$ is shown in Fig. 7, as are the trajectories of three particles for a duration $\Delta t=1.88/\sqrt{\beta}$. Each particle is initially at the same velocity, which is higher than that of the lattice, and each particle is $\pi/2$ out of phase with respect to each other. The final velocities of the three trajectories are not equal, and thus we expect that for an ensemble of particles that are distributed over a range of velocities, the distribution will be smeared in velocity because some will be accelerated, while others will be decelerated. If particles could be introduced into the lattice at a single phase, they could be accelerated or decelerated without velocity dispersion. We have calculated the velocity distribution function for the case $\psi>1$. The ensemble was initially in thermal equilibrium, and we have integrated the collisionless Boltzmann equation as described above. Figure 8 is a time series that shows the evolution of a CH_4 distribution function at a temperature of 5 K for the case $\psi=2$ with the initial lattice velocity at -2.0 km/s. All other parameters are the same as in Figs. 5 and 6 except that the chirp is now $\beta=3.38\times10^{19}$ rad/s^2. The initially Gaussian distribution function is observed to spread into two components, as some of the distribution is accelerated and some is decelerated. At $\Delta t=0.61$ ns, the perturbed distribution is almost symmetric, and almost equal numbers of particles are decelerated and accelerated. At this time, the peak of the accelerated distribution is approximately equal to the lattice velocity.

VII. EXPERIMENTAL CONSIDERATIONS

Using Eqs. (1) and (6), and relating the electric field to the intensity of the optical lattice by $E_1E_2=Z_0I/n$, we can estimate the maximum average velocity that can be achieved by the trapped ensemble. For a given intensity, the maximum

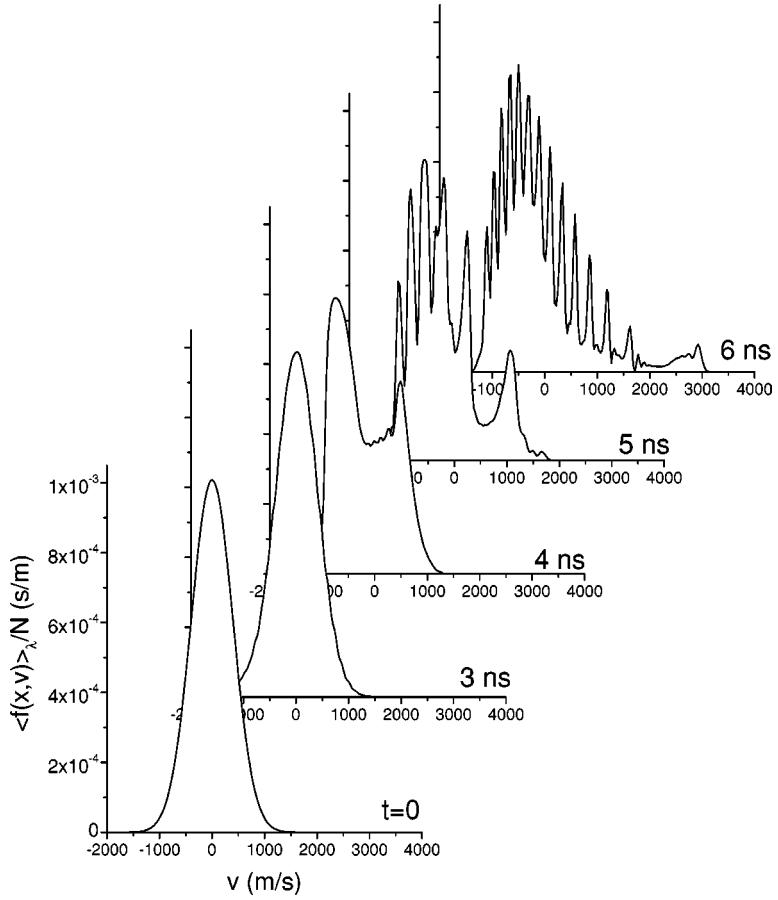

FIG. 6. The instantaneous velocity distribution function of CH_4 molecules perturbed by the lattice, for the case of $\psi=0.59$. The distribution at 0 ns, 3 ns, 4 ns, 5 ns, and 6 ns is shown. The distribution function was averaged over a spatial period of the lattice. No particles are trapped because the initial lattice velocity was -5 km/s. Although no particles are trapped, a significant number can be accelerated to near the lattice velocity over a short time period ($t<6$ ns).

chirp that can be applied to accelerate a trapped, polarizable molecule is given by

$$\beta<\frac{\alpha q^2 Z_0}{4nm}I, \tag{10}$$

where $Z_0=(\mu_0/\varepsilon_0)^{1/2}$, I is the available laser intensity derived from equal electric field amplitudes from each counterpropagating field, and n is the refractive index. From Eq. (2), and assuming a linear chirp with a top hat temporal profile, the maximum average velocity of a particular polarizable species is determined simply by the available fluence F and is given by

$$\zeta_{\max}<\frac{\alpha q Z_0}{2nm}F. \tag{11}$$

For example, CH_4 has a mass of 16 amu, and a polarizability of 2.9×10^{-40} Cm^2/V. If the lattice is formed by two 800 nm beams focused to 5 μm spot size (10 μm diameter), a maximum velocity of 20 km/s (33 eV) can be attained for 100 mJ beams, and 200 km/s (3.3 keV) for 1 J beams. A 100 mJ, 10-ns pulse corresponds to an intensity of 1.3×10^{17} W/m^2 (1.3×10^{13} W/cm^2) and thus the chirp must be less than 3.2×10^{19} rad/s^2. The laser must sweep over a frequency of 25 GHz within the 10 ns duration of the pulse, and acceleration occurs over a 100 μm distance. The production of chirped pulses over this spectral range on a 10-ns time scale is not routine, and therefore it appears that application of shorter, higher-intensity pulses with larger chirp may be more attractive. For example, an intensity of 1.3×10^{19} W/m^2 (1.3×10^{15} W/cm^2) from a 100 mJ, 100 ps laser pulse focused to 10 μm defines a maximum chirp of 3.2×10^{21} rad/s^2, and an acceleration distance of approximately 1 μm. This chirp may be produced by a picosecond transform-limited pulse that is stretched in time by group velocity dispersion within a Bragg fiber or by grating pairs. However, at this intensity, CH_4 and most other species, will be ionized. Therefore, to accelerate neutral particles, the maximum intensity that can be applied to molecules and atoms is, in practice, limited by ionization [23]. We note here that for all the numerical simulations performed in this paper, the intensity is below the ionization saturation intensity of the organic molecules measured in Ref. [23].

In Sec. V, we calculated the accelerated distribution using a top hat temporal profile so that the numerical calculations could be compared with the phase diagram for a constant value of ψ. For an experiment, it is instructive to investigate

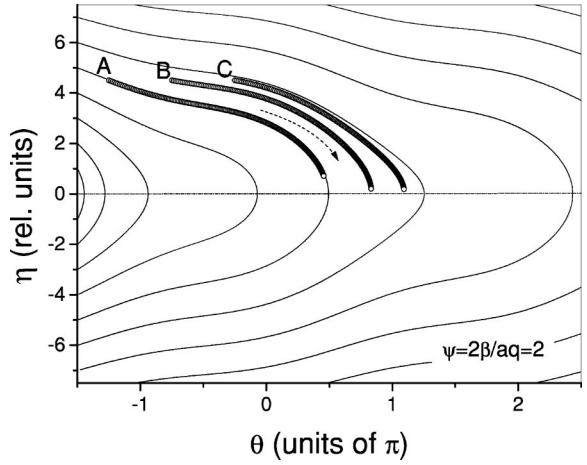

FIG. 7. The trajectories of three untrapped particles in the velocity phase space of an accelerating lattice, for the case $\psi=2$. The trajectories are for a duration of $1.88\beta^{-1/2}$. Each particle is initially at the same velocity, which is higher than the lattice velocity.

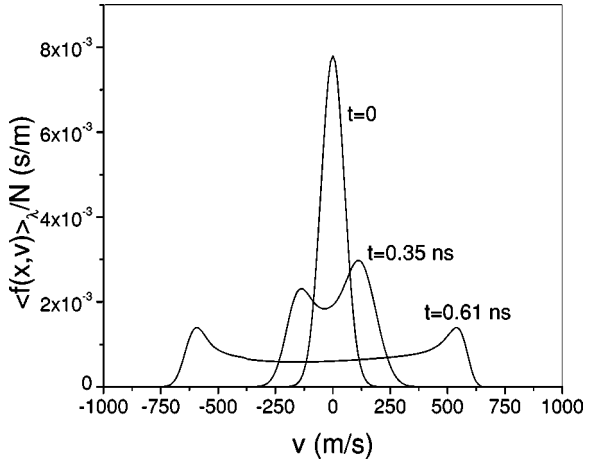

FIG. 8. The instantaneous velocity distribution function of CH_4 molecules in an optical lattice with $\psi=2$. The distribution at 0, 350, and 610 ps is shown, and each was averaged over the lattice period.

how a more realistic temporal profile can be used to accelerate an ensemble. For a Gaussian temporal profile, ψ and ΔU, the potential well depth, vary with time. Thus, for earlier times in the pulse when the intensity is low, few particles can be trapped when the initial velocity of the lattice is equal to zero. To accelerate particles using a Gaussian intensity profile, the initial velocity of the lattice must initially be negative so that, by the time the lattice has reached zero velocity, the potential is high enough to trap a larger number of particles that occupy this region of the velocity space. We have performed simulations with a Gaussian temporal profile with the same chirp as in Fig. 5, but starting with both zero and negative initial velocities. No appreciable accelerated distribution was produced for the zero initial veolcity case. Figure 9 shows the evolution of the ensemble of CH_4 molecules that are perturbed by a Gaussian temporal intensity profile with an initial lattice velocity of -5 km/s and chirp of $\beta=1\times10^{19}$ rad/s^2. The full-width half-maximum intensity of this Gaussian profile is 6.5×10^{15} W/m^2, which is the same as the top hat profile intensity in Fig. 5. As expected, the fraction of accelerated particles varies during the pulse because both ψ and the potential well depth ΔU vary during the acceleration period. In this case, at most 11% of the particles are trapped and accelerated compared to 30% for the top hat profile. The width of the accelerated distribution decreases as particles are lost from the lattice because the intensity rolls off in the latter part of the pulse. The number of particles in the long tail behind the accelerated distribution increases as these particles are lost from the lattice. Because we must start at a negative velocity, the final velocity that can be reached by starting at -5 km/s is approximately half that achieved by the top hat profile. These results indicate, that in an experiment, higher performance will be achieved for fields that can be rapidly switched on and off. The spatial variation of beam intensity must also be taken into account, since this will determine the number and spatial extent of the accelerated particles, as well as the variation in velocity across the beam. The spatial and temporal variation of the laser field will not change the essential physics of the acceleration process, but as shown above for the Gaussian temporal profile, they both must be considered to correctly model an experiment.

We have used exactly counterpropagating fields to model acceleration, but in practice, the two laser beams cannot exactly counterpropagate because the accelerated particles will impinge on one of the focusing optics. The angle between the beams must be less than 180°, but it should be maintained as close as possible to 180° to maximize both the lattice trapping force and the interaction region. We estimate that for a 5 μm Gaussian beam spot size (radius), a full angle of less than 174° will allow the accelerated beam of particles to pass the edge of the focusing optics. The change in the force per unit mass caused by this reduction in angle is less than 0.2%, and justifies our analysis using exactly counterpropagating beams. The Rayleigh range of the focused beams determines the upper limit to the acceleration distance, as well as the spatial extent of the accelerated group of particles. For a 5 μm spot size, this distance is approximately 200 μm, which is sufficient for the 100 ps, 100 mJ case discussed above. The maximum laser intensity that can be used will be limited by the probability of ionization with increasing intensity. These values have been tabulated for a number of molecules for an ionization rate of 10^6 s^{-1} [9].

We have used the static polarizability to describe the force on polarizable particles because, for many molecules, the laser sources available are far from resonance. However, for many atoms and some molecules, the laser sources can be tuned closer to resonance, and the force per unit mass provided by the optical field can be increased by at least an order of magnitude over the static case [7]. In these cases, the number of particles that can be trapped and accelerated can be increased, or the number of particles can be held fixed while increasing the final velocity of the accelerated distribution by increasing the chirp.

VIII. CONCLUSIONS

Optical potentials in the 10-100 meV range can be readily produced by high-intensity pulsed fields, and optical lattice

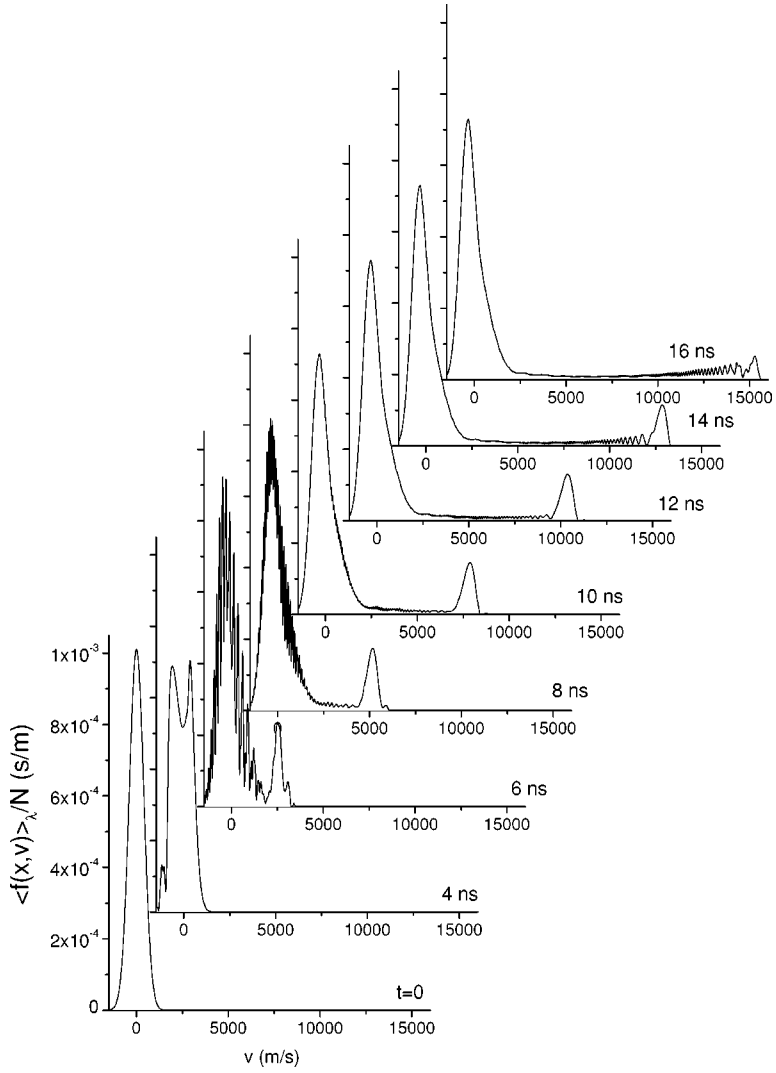

FIG. 9. The instantaneous velocity distribution function of CH_4 molecules within an accelerating optical lattice with a Gaussian temporal profile, in 2-ns time increments. The velocity distribution function was averaged over the spatial period of the lattice at each time period.

trapping forces per unit mass greater than 10^{12} m/s^2 can be achieved. Such large lattice forces are capable of trapping a large ensemble of particles so that high fluxes can be produced over nanosecond and subnanosecond time scales. This allows acceleration of a relatively dense ensemble of particles in the near absence of collisions. We have described the motion and acceleration of ensembles of polarizable particles, such as atoms and molecules, within these rapidly accelerating optical lattices. In particular, we have determined the conditions for collisionless acceleration of trapped and untrapped particles for the cases of $\psi<1$, and $\psi\geqslant 1$, which correspond to acceleration with and without a potential well, respectively. For $\psi<1$, we have derived expressions for the velocity of the trapped and accelerated distribution, as well as the velocity spread in terms of laser intensity and wavelength, and particle polarizability and mass. For the case of $\psi\geqslant 1$ we have predicted that both acceleration and deceleration can be produced in a potential for short time periods even though no potential well exists. Such accelerated distributions, which relax requirements on chirp, or the force per unit mass, may be more easily produced, and may be of use when a beam with a well-defined velocity (energy) is not required. Using CH_4 molecules as an example, we have predicted the temporal evolution of an ensemble of particles that are initially thermally distributed for both $\psi<1$ and $\psi\geqslant 1$ cases. We have discussed how the acceleration can be achieved in an experiment, and showed that for a particular species the maximum velocity is determined by the available laser fluence and pulse shape. Microlinear acceleration up to velocities in the 100-km/s range, over distances of less than 1 mm, may be used to produce neutral atomic and molecular beams with both higher velocities and densities than can be produced by pulsed molecular beams or other gas dynamic means. Our calculations have used the static polarizablility to determine the dipole force and therefore the predicted final velocities in this paper can be regarded as lower limits, since alignment of molecules within the field will result in larger optical forces. The final energy, and the spread

in energy, of the beam can be tailored by laser fluence, frequency chirp, and pulse duration. Such a configurable, intense, and compact source of high-energy neutral particles may find application to collision studies, lithography, and atomic and molecular implantation or etching.

ACKNOWLEDGMENTS

The authors would like to acknowledge many useful discussions with J. Grinstead, and Fiona Hinton for assistance with the manuscript.

[1] M.S. Livingston and J.P. Blewett, *Particle Accelerators* (McGraw-Hill, New York, 1962).
[2] A.J. Neely and R.J. Morgan, Aeronaut. J. **98**, 97 (1994).
[3] R.B. Miles, G.L. Brown, W.R. Lempert, R. Yetter, G.J. Williams, S.M. Bogdanoff, D. Natelson, and J.R. Guest, AIAA J. **33**, 1463 (1995).
[4] H.L. Bethlem, G. Berden, and G. Meijer, Phys. Rev. Lett. **83**, 1558 (1999).
[5] H.L. Bethlem, G. Berden, A.J.A. van Roij, F.M.H. Crompvoets, and G. Meijer, Phys. Rev. Lett. **84**, 5744 (2000).
[6] H.L. Bethlem, G. Berden, F.M.H. Crompvoets, R.T. Jongma, A.J.A. van Roij, and G. Meijer, Nature (London) **406**, 491 (2000).
[7] A.P. Kazantsev, Zh. Éksp. Teor. Fiz. **63**, 1628 (1972) [Sov. Phys. JETP **36**, 861 (1973)].
[8] A.P. Kazantsev, Zh. Éksp. Teor. Fiz. **66**, 1599 (1974) [Sov. Phys. JETP **39**, 784 (1974)].
[9] P.B. Corkum, C. Ellert, M. Mehendale, P. Dietrich, S. Hankin, S. Aseyev, D. Rayner, and D. Villeneuve, Faraday Discuss. **113**, 47 (1999).
[10] H. Stapelfeldt, H. Sakai, E. Constant, and P.B. Corkum, Phys. Rev. Lett. **79**, 2787 (1997).
[11] D.M. Villeneuve, S.A. Aseyev, P. Dietrich, M. Spanner, M.Y. Ivanov, and P.B Corkum, Phys. Rev. Lett. **85**, 542 (2000).
[12] K.W. Madison, C.F. Bharucha, P.R. Morrow, S.R. Wilkinson, Q.N.B. Sundaram, and M.G. Raizen, Appl. Phys. B: Lasers Opt. **B65**, 693 (1997).
[13] E. Peik, M. Ben Dahan, I. Bouchoule, Y. Castin, and C. Salomon, Appl. Phys. B: Lasers Opt. **B65**, 685 (1997).
[14] R.W. Boyd, *Nonlinear Optics* (Academic Press, Boston, 1992).
[15] H. Sakai, A. Tarasevitch, J. Danilov, H. Stapelfeldt, R.W. Yip, C. Ellert, E. Constant, and P.B. Corkum, Phys. Rev. A **57**, 2794 (1998).
[16] H. Sakai, C.P. Safvan, J.J. Larsen, K.M. Hiligsoe, K. Hald, and H. Stapelfeldt, J. Chem. Phys. **110**, 10235 (1999).
[17] J.J. Larsen, H. Sakai, C.P. Safvan, I. Wendt-Larsen, and H. Stapelfeldt, J. Chem. Phys. **111**, 7774 (1999).
[18] H.J. Metcalf and P. van der Straten, *Laser Cooling and Trapping* (Springer-Verlag, New York, 1999).
[19] J.H. Grinstead and P.F. Barker, Phys. Rev. Lett. **85**, 1222 (2000).
[20] P. Bhatnagar, E.P. Gross, and M. Krook, Phys. Rev. A **94**, 511 (1954).
[21] D.A. Anderson, J.C. Tannehill, and R. Fletcher, *Computational Fluid Mechanics and Heat Transfer* (Hemisphere Publishing, New York, 1984).
[22] D.R. Lide, *CRC Handbook of Chemistry and Physics* (CRC Press, Boca Raton, 2000).
[23] S.M. Hankin, D.M. Villeneuve, P.B. Corkum, and D.M. Rayner, Phys. Rev. Lett. **84**, 5082 (2000).